DESIGN AND CHARACTERIZATION OF A MICROFLUIDIC SYSTEM FOR SCANNING TRANSMISSION ELECTRON MICROSCOPY

By

Elisabeth Ariel Ring

Thesis

Submitted to the Faculty of the

Graduate School of Vanderbilt University

in partial fulfillment of the requirements

for the degree of

MASTER OF SCIENCE

in

Chemical and Physical Biology

August, 2010

Nashville, Tennessee

Approved:

Professor David Piston

Professor Niels de Jonge

Professor Phoebe Stewart

ACKNOWLEDGEMENTS

I would like to thank R.K.P. Benninger, M.J. Dukes, C.J. Easley, G-J Kremers, and D.B. Peckys for discussions and help with the experiments, W. Bigelow and R. Dona for help with mechanical design. The silicon microchips were designed in collaboration with Protochips Inc. (NC). The specimen holder was designed in collaboration with Hummingbird Scientific (WA). A Portion of this research was conducted at the SHaRE User Facility, which is sponsored by the Division of Scientific User Facilities, Office of Basic Energy Sciences, U.S. Department of Energy. This work was supported by Vanderbilt University Medical Center.

I am especially grateful to my mentor, Niels de Jonge for all of his time, help, and guidance. I am likewise grateful to Dave Piston, my co-mentor, for introducing me to this program, to imaging research, and to graduate studies in general. More thanks go to Al Beth, Hassane Mchaourab, and Lindsay Meyers for their essential assistance in navigating the Chemical and Physical Biology Program, and to Phoebe Stewart, for guidance through participating in my Thesis Committee, and inspiration as a successful woman in science. I am thankful to all whom I have had the pleasure to work with, in laboratory rotations, classes, and training programs.

Finally, I would like to thank my friends and family who have supported me at every step along the way. I could not have done any of this without them.

TABLE OF CONTENTS

Page

LIST OF TABLES

Table Page

LIST OF FIGURES

LIST OF ABBREVIATIONS

ADF ..... Annular Dark Field

CLEM ..... Correlative Light and Electron Microscopy

EGF ..... Epidermal Growth Factor

EGFR ..... Epidermal Growth Factor Receptor

EM ..... Electron Microscope/Microscopy

FWHM ..... Full Width at Half Maximum

HBSS ..... Hank's Balanced Salt Solution

LM ..... Light Microscope/Microscopy

PALM ..... Photo-Activated Localization Microscopy

PBS ..... Phosphate Buffered Solution

PDMS ..... Polydimethylsiloxane

QD ..... Quantum Dots

SEM ..... Scanning Electron Microscope/Microscopy

SiN ..... Silicon Nitride

STED ..... Stimulated Emission Depletion

STEM ..... Scanning Transmission Electron Microscope/Microscopy

STORM ..... Stochastical Optical Reconstruction Microscopy

TEM ..... Transmission Electron Microscope/Microscopy

CHAPTER I

INTRODUCTION AND BACKGROUND

To understand cellular processes on a molecular level, one must be able to examine the dynamics and interactions of individual proteins, which are on the scale of nanometers. The diffusive and direct motion of proteins within the cell, as well as their localization and interaction with other proteins and other biomacromolecules are all essential clues to the individual protein's function. The most straightforward way to obtain this information is by imaging the motion, localization, and interactions of proteins directly.

Currently, confocal laser scanning microscopy and fluorescence microscopy are the standard techniques for imaging intracellular processes within live biological samples in their native environment [1]. However, the spatial resolution of optical microscopy techniques is fundamentally limited to several hundred nanometers by diffraction. The spatial resolution of a system defines how close together two objects or features can be where they are still discernible as two distinct objects or features in an image. Abbe's diffraction limit [2] states that:

$$R = \frac{\lambda}{n \sin(\theta)} \tag{1}$$

where R is the resolution, λ is the wavelength of light used for imaging, n is the index of refraction, and θ is half-angle of the maximum cone of light that can enter the lens.

Because the maximum angle is 90 degrees, and the highest index of refraction in common optical equipment is about 1.5 [3], this leaves the optical system limited by the wavelength of light used, with lower wavelengths providing for higher resolution.

New ultra-high resolution optical techniques, sometimes called “nanoscopy” [4], such as stimulated emission depletion (STED) microscopy [5] and stochastical optical reconstruction microscopy (STORM) [6] have been shown to break Abbe’s diffraction limit of resolution, and can be used to obtain fluorescence images of cells, with a practically useable resolution on the order of 50 nm. Even higher resolution is possible with photo-activated localization microscopy (PALM) [7], but only with imaging times on the scale of hours, making real time imaging of highly dynamic systems impossible. Other imaging techniques that do not rely on visible light, such as X-ray crystallography can be used to obtain images of biological samples, with atomic resolution [8]. However, the sample must first be crystallized, which can be a difficult process that is not always possible with all samples of interest, and cannot be used to image dynamic events [9]. Electron microscopy can provide nanometer resolution of biological samples, but requires sample fixation, freezing, and/or slicing, making it impossible to image a sample in its native environment, or image dynamic events[10, 11].

There are several requirements to be fulfilled for successful high-resolution imaging of biological samples, where high-resolution is defined as <10 nm. Those requirements include the ability to:

- Image single proteins or other macromolecules
- Image in liquid
- Image in three dimensions
- Image the entire sample
- Determine where the particles of interest are located in relation to other features in the sample
- Image dynamic systems
- Image the interior of a sample
- Easily reproduce results

Ideally, one would wish to combine the high resolution of electron microscopy with the capabilities of light microscopy, allowing for real time imaging of a sample in its native, liquid environment. However, this is difficult, as electron microscopy (EM) is conventionally conducted in a vacuum.

There are several different types of electron microscopes. They are mainly classified as scanning electron microscopes (SEM), or transmission electron microscopes (TEM). A SEM images the surface of a sample by raster scanning a focused electron beam over the sample, detecting secondary, or backscattered electrons. A TEM image is created by passing a beam of electrons through a very thin sample. The beam interacts with the sample, and the resulting image is focused onto an imaging device.

Scientists have been working towards high resolution EM imaging in liquid for decades [12]. Two different types of specialized EM compatible liquid enclosures were developed in the early 2000's leading to a spatial resolution approaching 100 nm resolution in low-contrast stained cellular material, and 10 nm on high contrast materials in water - one for an SEM [13] and one for a TEM [14]. Alternatively, a specimen in a hydrated state can be imaged in an open wet environment, containing vapor and liquid, with a SEM [15] and a TEM [16, 17]. Recently, an improved very thin liquid enclosure led to nanometer resolution in a TEM [18].

The drawbacks of both these EM methods are that the SEM only images the surface of a sample, meaning one cannot obtain useful information from the interior of a whole cell; and the TEM can only image through samples that are thinner than about 0.5 micrometer. This is much thinner than a eukaryotic cell, which is typically ~5-10 μm thick [19]. Our group aims to overcome these drawbacks in order to image nanoparticles on the exterior and interior of a **whole** eukaryotic cell in liquid with nanometer resolution.

One way to overcome the inability to image the interior of the cell as well as the limitation on the thickness of the sample is to use a scanning transmission electron microscope (STEM). This is a type of TEM, meaning that the electron beam passes through the entire sample, however, the beam is focused and raster scanned over the sample as with a SEM. A typical STEM is shown in Figure 1.

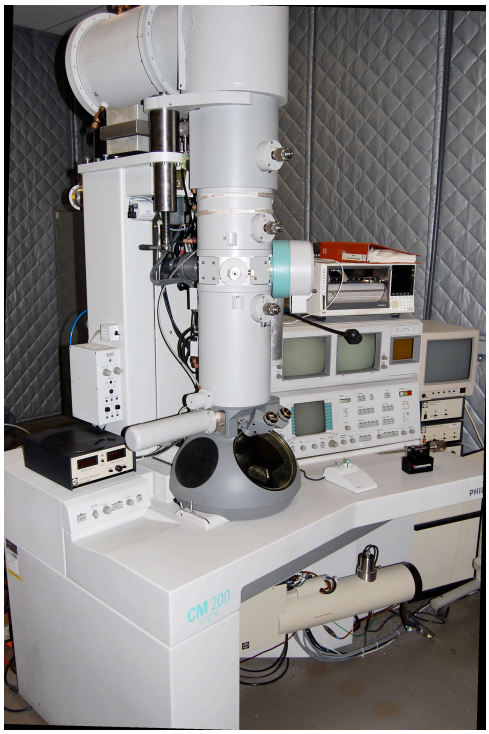

Figure 1 Philips CM 200 TEM/STEM.

In STEM imaging, as the beam passes through the sample, elastically scattered electrons are generated in proportion to the atomic number (Z) of the atoms in the sample [20], which creates a so-called Z-contrast, where the contrast of the resulting image varies with ~Z^2.

Those scattered electrons are collected by an annular dark field (ADF) detector. The number N of scattered electrons is calculated using the partial cross section for elastic scattering $\sigma(\beta)$. For the material thickness T, this number is given by [21]:

$$\frac{N}{N_0} = 1 - \exp\left(-\frac{T}{l}\right) = 1 - \exp\left(-z\sigma(\beta)\rho N_A / W\right), \tag{2}$$

with N_0 as the number of incident electrons, mean-free-path length for elastic scattering l, mass density ρ, the atomic weight W and Avogadro's number N_A,. The partial cross section for elastic scattering can be estimated by integrating the differential cross section $d\sigma/d\Omega$ assuming a simple screened Rutherford scattering model based on a Wentzel potential [21]:

$$\sigma(\beta) = \frac{Z^2 R^2 \lambda^2 \left(1 + E/E_0\right)^2}{\pi a_H^2} \frac{1}{1 + \left(\beta/\theta_0\right)^2} \tag{3}$$

$$E_0 = m_0 c^2; \lambda = \frac{hc}{\sqrt{2EE_0 + E^2}}; \theta_0 = \frac{\lambda}{2\pi R}; R = a_H Z^{-1/3}; E = Ue, \tag{4}$$

with electron accelerating voltage U, atomic number Z, the Bohr radius a_H, the rest mass of the electron m_0, the speed of light c, Planck's constant h, and the electron charge e. We chose settings of $\beta = 70$ mrad and $U = 200$ kV. So, we find that $l_{gold} = 73$ nm. For the water medium it follows that $l_{water} = 11$ μm using the average Z number of water of 4.7 [22]. The minimum particle height z that can be detected within a water layer of thickness T given a certain amount of electrons is [23]:

$$z = 5\, l_{gold} \sqrt{\frac{2T}{N_0 l_{water}}} \quad . \tag{1}$$

The value of z can be considered to be the sample-related resolution of liquid STEM imaging of a nanoparticle in a liquid layer. For gold nanoparticles and typical electron microscope settings (probe size = 1 nm and pixel dwell time is 20 μs) it follows that z = 1.3 nm for T = 5 μm [23].

This system is capable of imaging through a whole eukaryotic cell, as it provides contrast on nanoparticles made of high-Z materials, such as gold, which can be used as specific protein labels, embedded in several micrometer thick layers of low-Z materials, such water and cellular material. Gold nanoparticles are widely used in electron microscopy for specific protein labeling [24]. This capability can be used for the imaging of, for example, protein distributions in whole cells in their native liquid environment.

It is important to note that the resulting STEM images look different from TEM images, and are more useful for different types of images. TEM images can show high detail of cellular structure, but only for cells that have been fixed and thinly sectioned. STEM does not provide contrast between intracellular material, but instead provides high contrast on high-Z labels embedded in cellular material. An example of a TEM image and STEM image are shown in Figure 2.

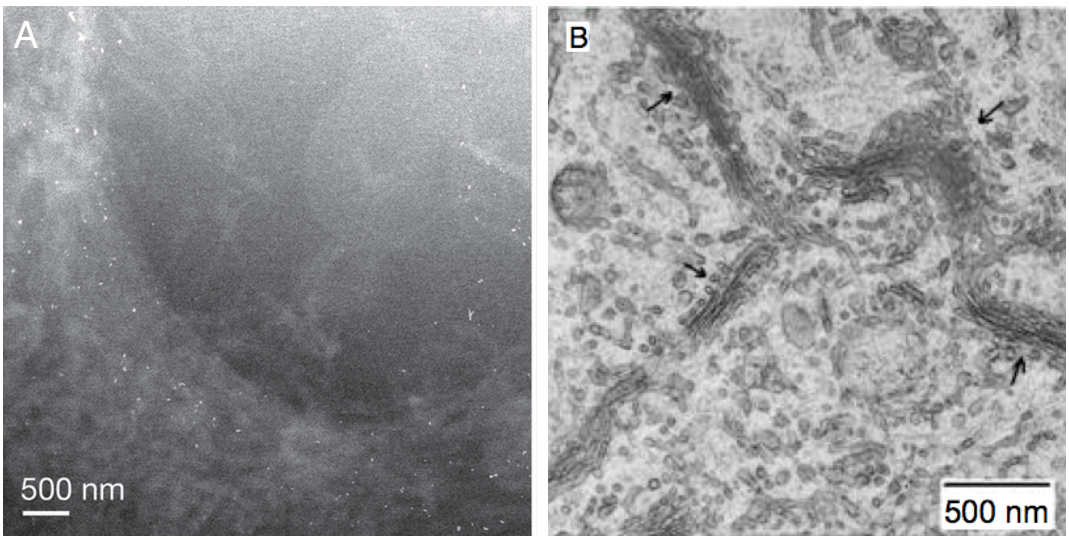

Figure 2 Illustration of the difference between STEM and TEM images (A) STEM Image of the edge of a fixed COS7 cell after 5-min incubation with EGF-Au. The labels are visible as bright spots and the cellular material is shown as light-gray matter on a dark-gray background. Note that there is little contrast in the cellular material, but the gold labels are of interest [23]. (B) TEM image of the Golgi apparatus in a cryo-prepared thin section from a stained COS7 cell. Note the contrast within the sample itself [7].

The de Jonge Laboratory has recently demonstrated that gold-tagged proteins can be imaged with 4 nm resolution in whole eukaryotic cells in liquid [23]. To image a sample in liquid in an electron microscope, the sample must be separated from the vacuum of the microscope. This is accomplished by enclosing the sample in a microfluidic device, which maintains a vacuum seal around the sample.

The microfluidic device consists of 2 microchips with thin silicon nitride windows. The windows are electron transparent and 50 nm thick. The microchips are biocompatible and cells can be grown directly on them. The microfluidic device is assembled by placing two of these chips with a thin spacer layer between them into a custom designed specimen holder for the electron microscope. The specimen holder, which can be used with current light and electron microscopes, includes input and output ports and microtubing to allow for fluid flow through the microfluidic device when the

tubing is connected to a syringe and pump. A schematic of the microfluidic system is shown in Figure 3.

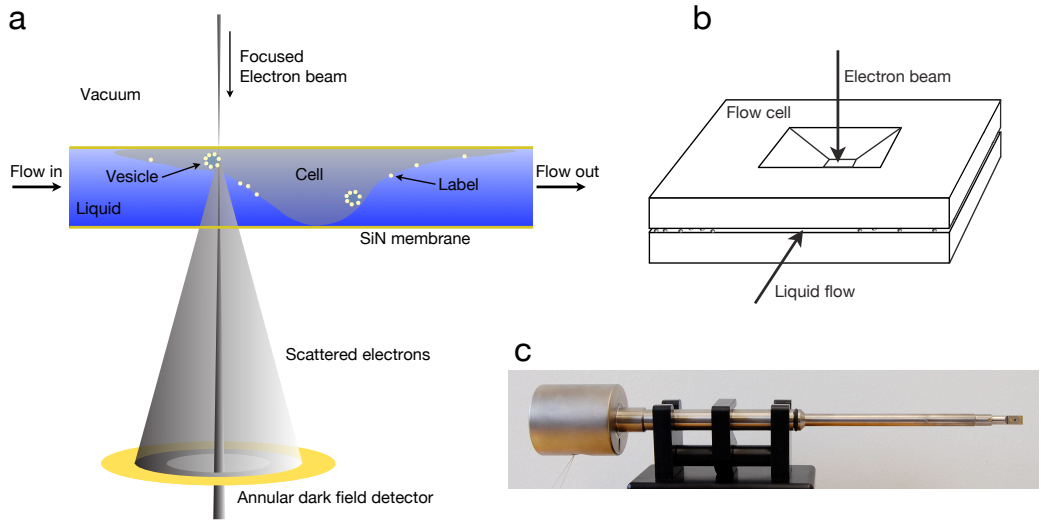

Figure 3 Schematic of the microfluidic system for liquid scanning transmission electron microscopy. (a) The liquid with nanoparticles is enclosed between two electron-transparent SiN windows, forming a channel for liquid flow. The enclosure is placed in the vacuum of the microscope. Images are obtained by scanning the electron beam and detecting elastically scattered transmitted electrons in the annular dark field detector. The dimensions and angles are not to scale. (b) Isometric schematic of the microchips outside of the sample holder. (c) Photograph of the entire holder. The tubing seen on the left hand side is connected to a syringe placed in a nanopump. [23]

The field of microfluidics has developed rapidly in the past decade, and developed from the general trend of miniaturization of electronic devices [25]. First examined as simply a way to miniaturize standard fluid delivery devices, such as pumps and sensors, one of the current strengths of microfluidic devices is for use in the biological sciences. Microfluidic devices can be used to more accurately model *in vivo* systems, because cells are allowed to grow in a more native-like state, with high cell densities, with constant influx of nutrients, and removal of waste [26]. Microfluidic devices can also minimize the amount of expensive sustaining media, or experimental reagents needed for biological

experiments. The use of microfluidic devices in electron microscopy (EM) is novel, as samples for EM are typically fixed, and thus do not require fluid flow.

The previously published work from the de Jonge group [23] relied on flat microchips separated by polystyrene microspheres, which was sufficient to obtain nanometer resolution images of labels in a whole cell while fluid was flowing through the system. However, we sought to improve this system, such that the flow through the system could be controlled, so that one could inject a particular fluid (media, drug, reagent, label, etc), and know precisely when that fluid would reach the sample, and how long it would take to saturate the sample. We also wanted to ensure that the fluid could be exchanged in a timely manner, on the scale of seconds or several minutes.

To achieve this goal, microchips were fabricated that included a 6 μm spacer layer made of SU-8 photoresist, creating a defined channel between the chips. The chips are placed in a slot in a custom designed specimen holder, where the slot is slightly bigger than the chips. Liquid flows through the main channel, and also though this extra space between the edge of the chips and the wall of the slot. That space acts as a bypass channel. The bypass channel is larger than the main channel between the chips, meaning most of the liquid will flow thorough the bypass channel, allowing for liquid to be exchanged in the system rapidly. Because this system has two well defined channels, rather than the unknown profile provided by the gap created using polystrene microspheres, the flow through the device (and specifically through the main channel) can be modeled.

In Chapter I of this thesis, I have presented a background of past progress in the field of imaging and specifically towards Liquid STEM. In Chapter II I will describe the

microfluidic system our group has developed, including the microchips and the liquid flow specimen holder. I will describe the methods used to grow cells on the microchips, and also describe results obtained by imaging the flow of microspheres in liquid through the system using light and electron microscopy. In Chapter III I will describe the calculations used, including determining the Reynolds Number of the system, determining the media requirements for cells growing in the device, and theoretical results obtained from developing a model to characterize the flow through the system, as well as from a model for Brownian motion of small particles in the device. In Chapter IV, I will state the results of the cell seeding, and light and electron microscopy experiments, and I will discuss the implications of those results in Chapter V. The details of the light and electron microscopy experiments and flow characterization (parts of Chapters II-V) have recently been accepted for publication in *Microscopy & Microanalysis* [27]. I will provide a summary of the thesis in Chapter VI, finishing with some future directions for the research in Chapter VII.

CHAPTER II

METHODS

Microchips

The key component of the liquid STEM system was a microfluidic chamber consisting of two custom designed silicon microchips, each supporting a 50 nm thick silicon nitride (SiN) window (Protochips, Inc., NC) [23]. This chamber was placed in the vacuum of the electron microscope, while being connected to the outside of the microscope at atmospheric pressure or greater via plastic tubing. The SiN windows reliably withstood this pressure difference, as was also concluded by others for thinner windows [28].

The dimensions of the microchip were 2.00 × 2.60 × 0.30 mm, and those of the SiN window were 50 × 200 μm. All tolerances were ±10 μm, except for the thickness of the microchip; this tolerance was ±30 μm. The windows, see Figure 4, were defined by photolithography from the backside of the microchips using a KOH etching process. The edges of the microchips were manufactured with a precision of ±10 μm with respect to the SiN window position to allow precise alignment of the windows in a stack of two microchips as needed to form the micro-fluidic chamber. The microchips were diced with a saw that was guided by etched grooves in the silicon wafer. Figure 4c shows the smooth edge surfaces obtained with dicing.

The thickness of 50 nm of the SiN window was chosen because SiN of this thickness causes negligible electron beam broadening in the STEM at 200 kV. The

typical gold fringes, indicating a resolution better than 0.2 nm, were visible for the nanoparticles at both sides. The dimensions of the windows were chosen such that several eukaryotic cells of typical size would be visible through the window, while keeping the window size to a minimum to avoid excessive bulging of the windows when the microfluidic chamber, with its interior at atmospheric pressure was placed in the vacuum of the electron microscope. The maximum bulging of the window was found to be 1 - 1.5 μm, such that the microfluidic chamber was 2 - 3 μm thicker in the middle of the window than at its edge. A window of 70 ± 10 μm width was also tested and the bulging was found to be 2 - 3 μm.

A microfluidic chamber was assembled by placing two microchips on top of each other with their SiN sides facing. Previously, the chamber was constructed of two flat chips. Polystyrene microspheres were positioned at the four corners of one microchip, by pipetting 0.2 μl droplets of water containing microspheres on the microchip while the surface was hydrophobic. The liquid stayed as droplets at the four corners, instead of wetting the surface, then evaporated, leaving microspheres deposited in the corners. Because the user could select what size microspheres to use, the depth of the gap was customizable.

However, the system did not allow for precise characterization of flow, because there were not well defined channels – just an open space separated by microspheres. In order to create defined channels, instead of two flat chips, a fixed spacer layer was manufactured from SU8 material directly on the microchips, see Figure 4 b, c, and d. The chamber was then assembled using one flat chip, and one of the microchips that contained a spacer, typically with a 6 μm thickness, such that liquid could flow between

the microchips, and to provide a specimen chamber with sufficient height to contain thin eukaryotic cells, for example, COS7 fibroblast cells.

The spacer defined a flow channel over the long side of the microchip. The spacer consisted of a wall with a void in its middle to provide space for debris and cellular material when two microchips were pressed together to form a micro-fluidic chamber. The wall did not extend to the very edge of the microchip to avoid delaminating during dicing. Different spacer models were developed, providing for channels with varying widths. Models were also developed with beveled edges, such that rather than flatten any cellular material between the chip and the spacer, they might slice through the material. Details of the microchips are shown in Figure 4.

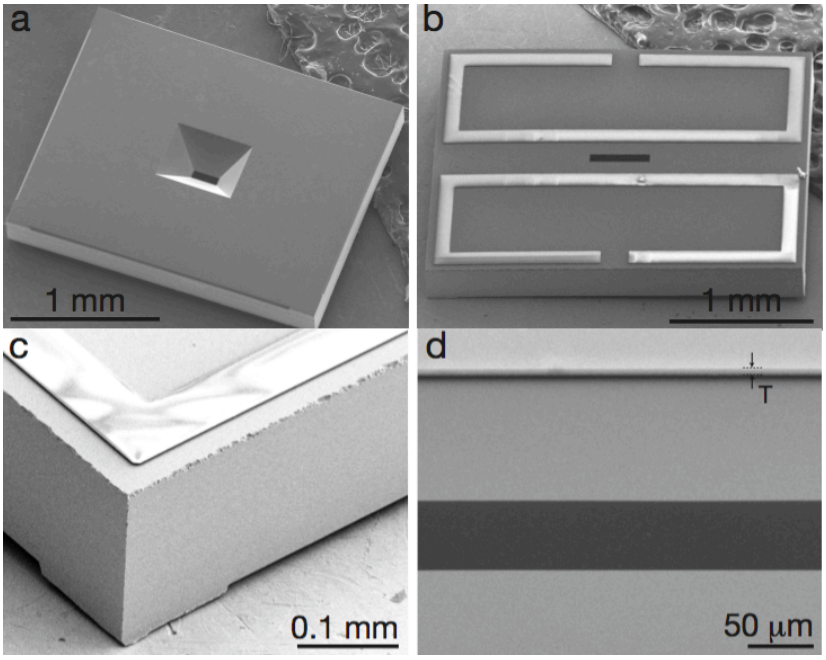

Figure 4 Scanning electron microscopy (SEM) images of the microchips. The SEM images were recorded at 10 kV (S4700 Hitachi). (a) Image of the backside of a microchip showing the opening for the silicon nitride window. (b) Image of the silicon nitride side of the microchip showing the shape of the SU8 spacer; charging effects distort the image at the positions of the spacer. The silicon nitride window is the dark shape. (c) Close-up of the edge of the microchip showing the precision-diced edges. The corner of the SU8 spacer can be seen on top of the microchip. (d) Close-up at the position of the silicon nitride window of the spacer microchip, recorded at 45° tilt. The thickness of the spacer layer T was measured to be 6.1 µm. [27]

The microchips were manufactured with a protective coating of resist, which was stripped with acetone and ethanol prior to usage. New microchips were found to be hydrophobic. For optimal liquid flow and for work with cells, we tested several cleaning methods, and different chip coatings and cell placement/growth environments.

Cell Seeding Experiments

In order to minimize the effort required to seed cells on the chips for imaging experiments, we experimented with different methods:

1) pipetting detached cells onto the chips and allowing them to attach to the surface of the chips, and

2) culturing the cells directly on the chips.

For the first method, we placed a 2.5 μL droplet of suspended cells in the middle of a clean chip. We then placed the chip in an open Petri dish within a beaker of water and placed the beaker in a 37 ^{o}C incubator. After ~30 minutes, the chip was transferred to a vial with media and allowed to grow for ~2 more hours.

For the second method, we followed the typical cell culture protocol, but instead of culturing the cells in flasks, we cultured them in Petri dishes with a layer of the organic polymer polydimethylsiloxane (PDMS) on the bottom. The stickiness of the PDMS kept the chips attached to the bottom of the dish, instead of floating around. This kept the chips from being damaged, as well as encouraging normal growth over the entire bottom surface of the dish, including the tops of the chips. We tested both a plain PDMS layer, as well as layer of PDMS coated with Pluronics F127. This was tested to see if the Pluronics would discourage cell growth on that layer, thus encouraging cell growth on the chips.

Furthermore, we experimented with different coatings on the chips. We tested plain, clean chips, clean chips that had been plasma cleaned (to cause the surface of the chips to become hydrophilic), clean chips that were coated with poly-L-lysine (to improve chances for cell adhesion), and clean chips that were plasma cleaned and coated with poly-L-lysine (to improve chances for cell adhesion, and increase the length of time that the chips remained hydrophilic).

Twenty-four chips were cleaned in acetone, water, and then ethanol, and 12 were plasma cleaned for about one minute. Six of the plasma cleaned chips and 6 of the plain chips were coated with 5 μL per chip of poly-L-lysine for ~1 hr, and then rinsed with Hank's Balanced Salt Solution (HBSS.) Four Petri dishes with a layer of PDMS at the bottom were prepared, and 2 of those dishes were coated with a 1:1000 solution of HBSS and Pluronics F127 for 1 hr, and then rinsed with HBSS. The chips were split evenly between the Petri dishes with 3 of each type of chip exposed to both kinds of dishes. The preparations and coatings tested are summarized in Table 1.

Table 1 – Summary of how many of each chip preparation were tested, and in what kind of Petri dish.

	PDMS	PDMS coated in Pluronics
Plain	3	3
Plasma cleaned	3	3
Poly-L-lysine	3	3
Plasma cleaned + Poly-L-lysine	3	3

Each dish was filled with 3 mL of freshly split cells in media, and allowed to incubate overnight. The next day the chips were imaged in a light microscope, and the number of cells visible in each window were counted by hand.

Specimen Holder

The microfluidic chamber was assembled in the tip of a custom built specimen holder (Hummingbird Scientific, WA) providing, 1) liquid flow to and from the specimen chamber to the exterior of the electron microscope, 2) vacuum sealing of the liquid-exposed regions of the system, and 3) alignment of the two microchips. Schematic drawings are shown in Figure 5.

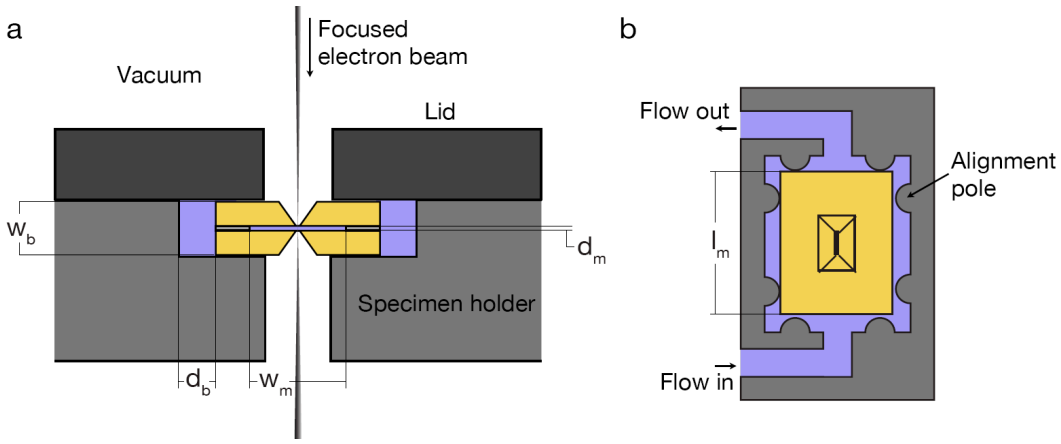

Figure 5 Schematic drawings of the tip of the specimen holder for liquid STEM. These drawings do not reflect the exact dimensions of the specimen holder. (a) Side-view cross-section. The silicon microchips are placed in a slot at the tip of the specimen rod. A lid with screws closes the slot. (b) Top view of the slot showing the alignment poles, position of the microchips, and the liquid flow path. [27]

The tip contained a slot fitting the two silicon microchips and was closed by a lid with screws. Bores in the tip and lid exposed the SiN windows to the electron beam in the vacuum. Three small O-rings, two at the top and one at the bottom of the stack of

two microchips provided the vacuum seals. All O-rings were coated with a thin layer of vacuum grease. Channels in the slot connected the liquid in the specimen region to the input and output tubing. Microfluidic tubing (PEEK tubing with an inner diameter of 50 μm, Upchurch Scientific) was fed through holes in the specimen holder connecting to the slot, and was held in place by epoxy (Torr Seal, Varian).

For precision alignment the microchips were placed in the slot and then pushed flush with a minimum of three rounded alignment poles, see Figure 5b. Rounded surfaces provide contact points. The gap between the remaining poles at the other side of the slot and the microchips was about 30 μm. The gap was needed to allow loading the microchips, and also provided a bypass channel for the liquid. In this system most of the liquid was pumped around the microchips, such that the liquid in the entire system could be replaced rapidly. The microfluidic tubing was connected to a 1 mL glass syringe (Hamilton) in a syringe pump (Pico Plus, Harvard Scientific). Figure 6 shows a photograph of the specimen holder and the liquid handling system placed on a STEM.

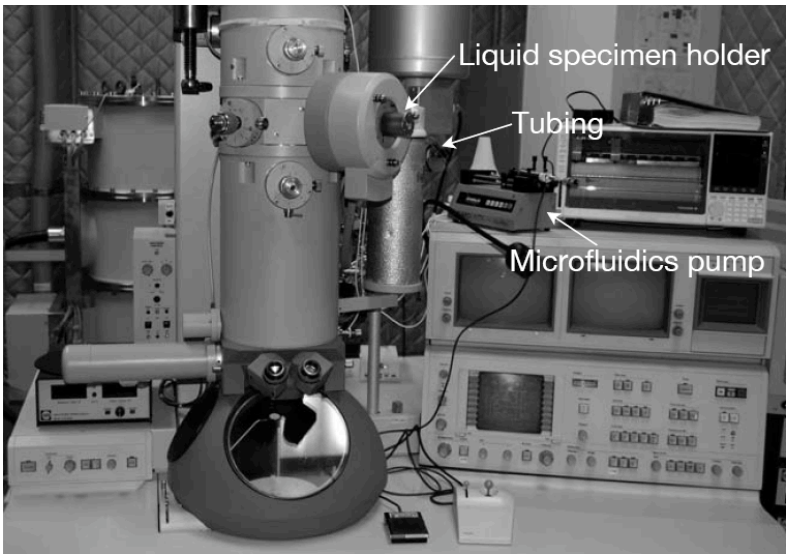

Figure 6 Specimen holder for liquid STEM placed in the electron microscope (CM 200, Philips/FEI). The microfluidic tubing and the syringe pump are also visible.

It should be noted that the liquid STEM system presented here involves only three components (the microchips, specimen holder, and pump), transforming a standard STEM (or TEM) into an *in situ* system for imaging in liquid at atmospheric pressure, making the system easy to obtain and use in any STEM equipped laboratory.

Sample Loading Procedure

The microchips were loaded in the specimen holder with the following procedure. A new session always started with the cleaning of all tubing and the holder by flushing H_2O through both input and output tubing. Prior to specimen loading the slot was dried. A microchip with spacer was placed in the slot and a 0.5 μl liquid droplet was applied with a pipette (Eppendorf). The liquid was typically HPLC grade H_2O and 100 mM NaCl, or another salt buffer. The salt provided electrical conductance in the liquid to reduce charging effects caused by secondary electrons during STEM imaging. The second microchip was loaded while the first microchip was still wet. The microchips roughly aligned by themselves in the slot due to the interaction of the surfaces with the water drop, presumably by optimizing the liquid/chip wetting. The microchips were then pressed to one side with tweezers for fine alignment.

The lid was placed on top of the stack and the screws were tightened with a torque screwdriver to provide equal force on each screw. The pump was started with a volumetric flow speed Q = 5 μl/min and the microchips were inspected for leakage over a period of 5 minutes under a binocular. Broken SiN windows, or incorrect sealing on the O-rings led to the formation of liquid droplets on the outside of the microfluidics chamber. Testing in the STEM revealed that SiN windows could withstand Q = 5 μl/min

when the chamber was placed in the vacuum of the microscope, while a few cases of rupture were observed for Q = 10 μl/min. For electron microscopy we usually set Q = 2 μl/min.

Light Microscopy Experiments

The behavior of the liquid in the microfluidic chamber was tested by flowing polystyrene microspheres through the system and observing the flowing microspheres with a fluorescence microscope (TE300, Nikon, with Metamorph imaging software, Molecular Devices). A microfluidic chamber was assembled from one standard microchip, and one with a 6 μm thick SU8 spacer layer. There were no cells on either of the chips. We followed the above sample loading procedure, but used pure water instead of saline water. The experiment was conducted for two different sizes of microscospheres, 2.2 μm diameter (Polysciences, Inc), and 0.28 μm (Molecular Probes). Sonicated, diluted solutions of the microspheres in water were loaded in the syringe and the flow was started with Q = 5 μL/min. Note that it appeared to be necessary to initiate the flow with Q = 2 - 5 μL/min. The first microspheres appeared in the window about 4 minutes after starting the pump.

Sequence of images were recorded with exposure times of 50 ms per image, a total duration of 15 s, and an interval of 500 ms between images. Sequences were recorded after 5, 10, 20, and 30 minutes from pump start. The pump speed was then reduced to 2 μL/min and sequences of images were recorded ~0.1 , 10, 20, and 30 minutes after the speed change. This experiment was repeated for Q = 1 μL/min, 0.5

μL/min, and 0.2 μL/min, and then the rate was ramped back up through those settings to 5 μL/min. As a control we also recorded sequences of images for a static liquid.

Electron Microscopy Experiments

To test the system in the STEM, a flowing liquid containing gold nanoparticles was imaged with a STEM (200 kV, CM200 STEM/TEM, Philips/FEI Company). The microfluidic chamber was assembled from one standard microchip and one microchip with a 6 μm thick SU8 spacer layer. The windows did not contain nanoparticles prior to the experiment. The pump lines were first filled with 10% Phosphate Buffered Solution in water (PBS). A concentrated solution of 100 nm and 30 nm diameter gold nanoparticles in 10% PBS was then loaded in a syringe. The specimen holder was loaded in the STEM and the pump was started with $Q = 2$ μl/min. The microscope was set to a probe current of 0.58 nA, a detector semi-angle of 94 mrad, with a pixel dwell time of 5 μs, an image size of 512×512 pixels, and operated in continuous imaging mode. The electron beam scan direction was aligned to the long side of the flow cell.

CHAPTER III

CALCULATIONS

In order to use this system to test the effects of a liquid on a sample, one must be able to model the flow system mathematically, so that one knows exactly when the liquid reaches the sample, how long it takes before the liquid traverses across the entire sample, and how long it takes the liquid to reach the end of the output tubing, in case any further experimentation on the liquid is required. Before developing this model, we first had to ensure that we were working with a microfluidic system that was operating under laminar flow conditions. This is done by calculating the Reynolds number of the system [25].

Reynolds Number

The Reynolds number is a measure of the ratio between the inertial forces and the viscous forces in a particular flow system [25]. In typical macrofluidic systems, flow is non-laminar (ie inertial effects dominate viscous effects.) However, one unique aspect of most microfluidic devices is that the scale is such that flow is laminar. This is more important when dealing with devices of higher complexity, such as mixers, or systems with flows of more than one fluid. But it is also important to describe how fluid will interact with the cells and microspheres it encounters. Furthermore, laminar flow must be ensured in order to make comparisons with other known equations, which have only been confirmed in other laminar systems.

The Reynolds number is a dimensionless quantity given by

$$\mathrm{Re} = \frac{\rho u L}{\eta} \tag{6}$$

where ρ is the density of the fluid, *u* is the linear velocity, *L* is the characteristic length, and η is the dynamic viscosity. The linear velocity (u) can be determined from the volumetric velocity (Q), which is dialed into the pump. The linear and volumetric velocities are related as u = 4Q/wd, where w is the half width of the channel being investigated, and d is the half depth.

This value can vary greatly from system to system, however even using the uppermost limits that this system might see (i.e. a volumetric velocity on the scale of microliters per minute, vs the more typical nanoliters per hour), the Reynolds number comes out to 13.1. Reynolds numbers under 1500 are considered laminar [25], so this system qualifies.

Media Requirements

We also wanted to determine the amount of media that the cells in the device would require to survive during the assembly of the microfluidic device and transportation to the microscope. Consider that under normal conditions about 5 million cells (maximum) are kept in 6 mL of media, which is changed about every 48 hours. When those cells are split, about 5% of the cells are kept each time. So the average number of cells that require, 6mL of media over 48 hours is about 1,580,000. This shows that one cell would need at least about .08 nL per cell per hour.

For a chamber with the dimensions 2.50 mm by 1.26 mm by 6 microns the volume is 18.9 nL. However, because one of the chips is covered with cells, which are about 5 microns thick, the space available for media is only about 3.15 nL. If one cell needs about .08 nL/hour to survive, and in the space of an entire chip, we could expect up to about 6,300 cells to be growing, then without any flow, the cells of interest could survive for only a few seconds before they would start running out of media. This shows why a flow system is needed to continually refresh the media for the cells. The flow system can accommodate a flow rate on a scale of μL per minute, which is higher than required to keep the cells alive.

Flow Characterization/Modeling

To ensure that the system would be able to withstand the necessary flow rates, a model of liquid flow was developed for the microfluidic chamber and liquid bypass in the specimen holder with the purpose of predicting the speed of liquid fronts at the various positions in the system as function of the input flow set on the syringe pump. The microfluidic system can be modeled as an electronic circuit, as shown in Figure 7, with fluid pressure represented as voltage, flow rate represented as current, and fluidic resistance of the channels represented as electronic resistance.

The microfluidic system was approximated by a simplified volumetric flow model consisting of two channels, i.e., the main channel between the microchips, and a bypass channel along one side of the stack of the two microchips. It was assumed that both channels had a rectangular cross section and that the microchips were pressed to one side against the alignment poles, such that that liquid passed at one side only. It was further

assumed that liquid could enter both channels from a larger reservoir without resistance. Flow above and below the microchips was assumed to be blocked by the O-rings. The setup and its electronic representation are shown in Figure 7.

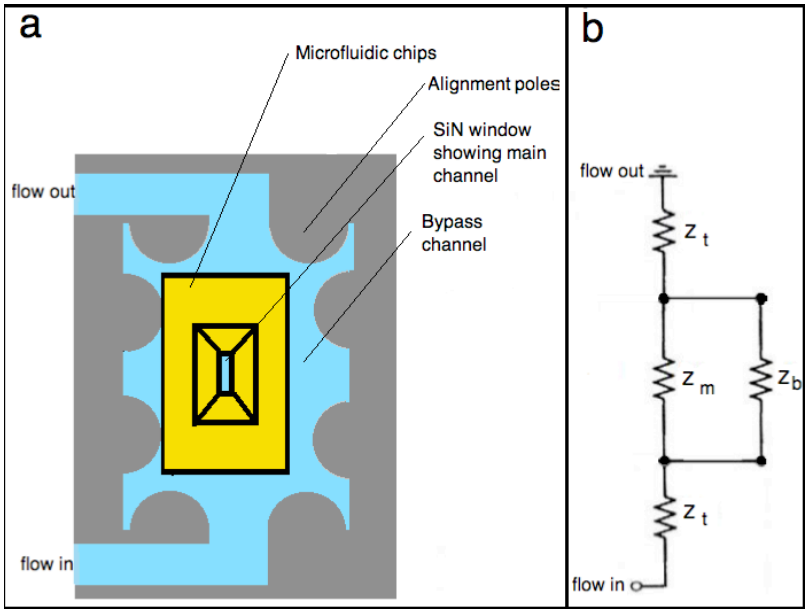

Figure 7 Schematic representation of microfluidic setup. (a) Schematic of actual setup. (b) Schematic of electronic representation of setup. The Z values represent Resistance, and the subscripts are t=tubing, m=main channel, b=bypass channel. Schematic not to scale.

The flow resistance Z of a channel was calculated using [29]

$$Z = \frac{4\eta l}{w^2 d^2 F} \quad , \tag{7}$$

with viscosity η (for water $\eta = 8.9 \times 10^{-4}$ kg·s^{-1}·m^{-1}), length of the channel l, width of the channel w, depth of the channel d ($d < w$). F is a form factor for a rectangular cross sectional channel [30],

$$F = \frac{w}{3d} - \frac{64w^2}{\pi^5 d^2} \sum_{n=0}^{\infty} \frac{\tanh\left[\frac{(2n+1)\pi d}{2w}\right]}{(2n+1)^5}, \tag{8}$$

To simplify the calculations, we used the following numerical approximation [31],

$$F \approx .0566\left(\frac{d}{w}\right)^3 - .262\left(\frac{d}{w}\right)^2 + .347\left(\frac{d}{w}\right) - .000699, \tag{9}$$

The volumetric flow Q through a device with a main- and a bypass channel was calculated using the current divider rule. The linear flow speed v (in m/s) in the main channel is then,

$$v = \frac{QZ_b}{d_m w_m (Z_m + Z_b)}, \tag{10}$$

with Z_m the flow resistance of the main channel and Z_b that of the bypass channel. The value of Q was known from the particular pump speed. The dimensions of the main channel were $d_m = h = 6$ μm, $w_m = 1.26$ mm and $l_m = 2.50$ mm, and the dimensions of the bypass channel were $w_b = 612$ μm and $l_b = l_m = 2.50$ mm.

Due to the alignment poles (Figure 5b) it was not possible to determine a precise value of d_b. The shortest distance between a pole and the microchip was measured to be 30 μm, while most of the channel had $d_b = 60$ μm. The flow resistance of the bypass

channel was, therefore, determined experimentally, assuming a flow channel with rectangular cross section and a representative average value of d_b. By using the experimental data with Equation (10) to find Z_b, then using Equation (7) to find d_b, it was found that d_b = 47 μm, which is indeed between 30 and 60 μm.

Using Equation (10), we were able to determine what the expected flow would be through the main channel of our system. Using the typical flow rate of 2 μL/min as the input flow rate, the flow rate through the main channel was found to be .02 μL/min. This is more than twice the flow rate required for the cells to survive.

This also shows that the bypass channel is essential for rapid exchange of liquid in the system (on the scale of seconds or minutes). Rapid liquid exchange is needed for experiments where, for example, the response of a cell to a certain stimulus is investigated. Stimuli can consist, for example, of a change of the chemical environment (pH, salt concentration, additional chemical substances, temperature), the introduction of a ligand for a certain receptor, or the injection of micro-, or nanoparticles, as separate particles, or with attached antibodies or ligands for specific protein labelling. The chemicals, or particles can be injected from the outside of the electron microscope. The experiment with the microspheres is in fact an example of such an injection.

For Q = 2 μL/min it can be calculated that the time from injection for a liquid front to reach the specimen region would be 1 minute, in case of tubing with a diameter of 50 μm and a length of 1 m. This highlights the role of the bypass channel, as without it, all liquid in the tubing would have to be replaced by flowing through the main channel, meaning the time span would be 6.3 hours.

Brownian Motion

Finally, we realized that because of the small size of the particles being examined, and because they would be in liquid, Brownian motion of the particles would be evident in our imaging. Brownian motion is always present for particles with sizes on the micron scale or smaller. The mean squared distance (i.e., the square of the distance a particle travels between two time points that a particle travels, not taking into consideration the path that particle took to get between the two points) is proportional to the time it took to travel that distance [32],

$$x = \sqrt{2Dt}\,, \tag{11}$$

where x is the distance travelled, D is the diffusion constant, and t is the time interval. D can be determined from,

$$D = \frac{k_b T}{6\pi\eta r}, \tag{12}$$

where k_B is Boltzmann's constant, T is the absolute temperature, and r is the radius of the particle.

We found that the 2.2 μm and 0.28 μm microspheres are thus expected to diffuse by x = 0.67 μm/s and 1.9 μm/s, respectively.

CHAPTER IV

EXPERIMENTAL RESULTS

The three main aspects of the microfluidic system that were tested were the preparation conditions for cell growth on the chips, the flow rate of fluorescent microspheres as measured in a light microscope, and the flow of gold nanoparticles as measured in a STEM. The first was to test the best way to grow/place the cells for future imaging In the experiments. The next experiments were both conducted as a way to characterize the fluid flow through the system. Furthermore, imaging the moving gold particles in the STEM served as a proof of concept, as moving particles in liquid have not been imaged in a STEM prior to this.

Cell Seeding Experiments

In testing the different chip preparations and growth conditions, we found no significant difference between the different coatings on the chips, and the coatings on the PDMS, as indicated by a P-value of 0.0987. The number of cells seen in the windows are summarized in figure 8a. We further compared whether coating the growth surface with the Pluronics F127 affected the cell growth, regardless of the coatings on the chip. We found slightly more cell growth when the surface was not coated, however this difference was insignificant, as indicated by the P-value of 0.2093. P-values less than .05 are deemed significant. These results are shown in Figure 8b.

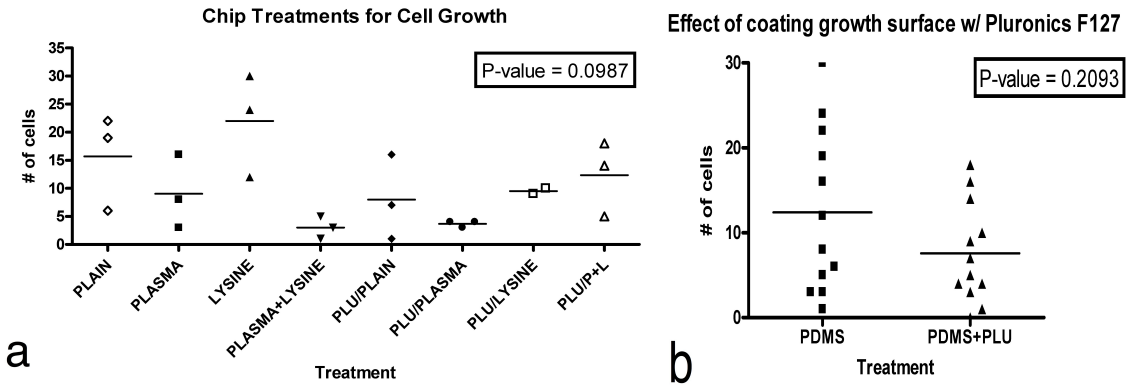

Figure 8 Figure showing summary of results of growing cells on differently treated chips on differently coated Petri dishes. (a) Results of all tests. (b) Summary, comparing only the effect of treating the dish with Pluronics F127. Statistically, all preparations were equal.

The light microscopy experiments served to show how closely the parallel-resistor model matched the actual measured flow rates in the microfluidic system. Furthermore, the experimental results allowed us to solve the parallel-resistor model for the unknown bypass channel depth dimension. They further acted as a demonstration of Brownian motion, and gave an idea of what to expect when looking for particles in the later STEM experiment.

Light Microscopy Experiments

For the LM experiments, the image sequences were analyzed by tracking the positions of the microspheres from image to image (using the MTrackJ plug-in for ImageJ). Representative samples of some of the results are shown in Figure 9.

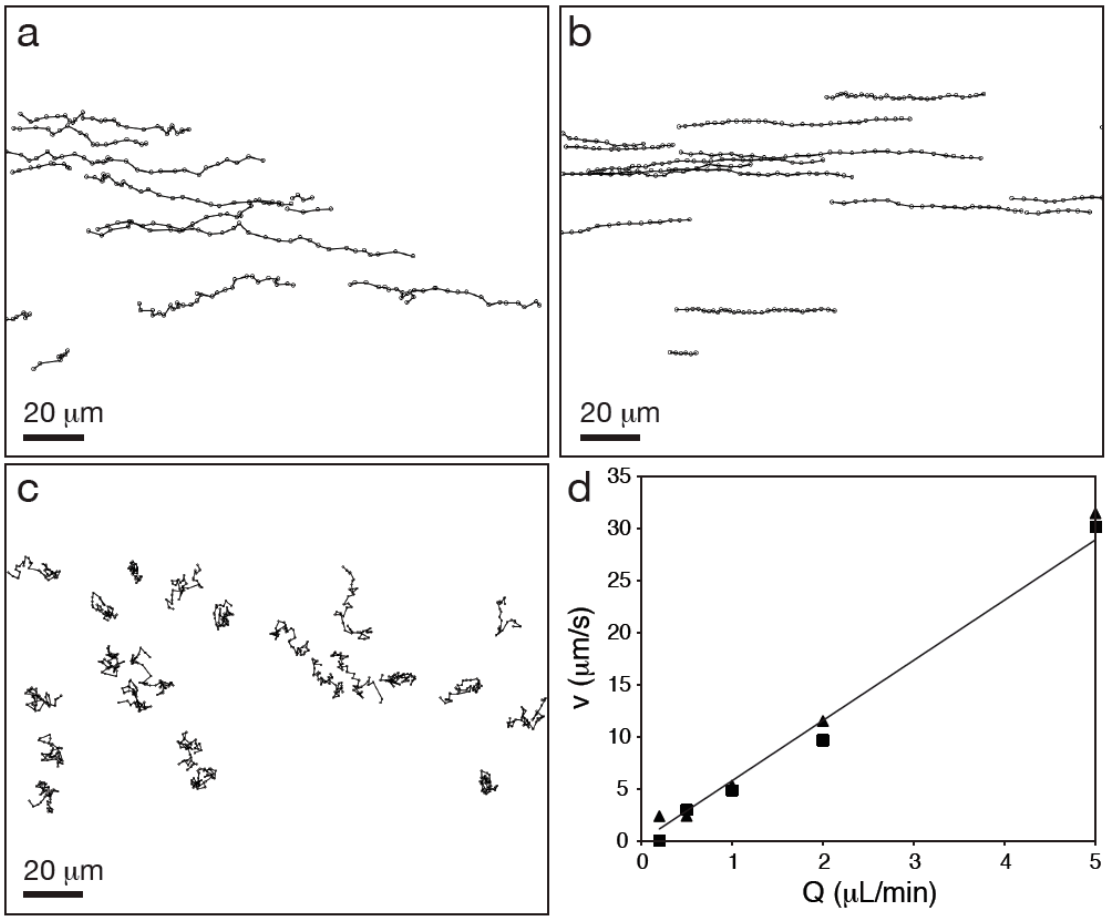

Figure 9 Analysis of the flow of microspheres through the microfluidics chamber with fluorescence microscopy. (a) Trajectories of 0.28 μm diameter microspheres visible through the silicon nitride window of the main channel at a pump speed of 1 μL/min. The figure is aligned with the long side of the channel, such that liquid flow is in horizontal direction. (b) Trajectories of 2.2 μm microspheres at 1 μL/min pump speed. (c) Trajectories of 0.28 μm microspheres in a control experiment with static liquid. (d) Measured flow speed *v* in the main channel as function of the pump speed Q, for 0.28 μm microspheres (squares) and 2.2 μm microsphere (triangles). The line indicates the calculated *v*, where d_b has been set to 47.3 μm to fit the data. [27]

Figures a and b shows the trajectories obtained at Q = 1 μL/min for both microsphere sizes. The flow of the microspheres was approximately aligned with the direction of liquid flow, which was in horizontal direction with respect to the figure. But, the trajectories also showed deviations, some were curved and several microspheres appeared to change their direction from time to time. The deviations from homogeneous

flow were more pronounced for the smaller microspheres than for the larger ones, and were more apparent at low speeds.

The trajectories recorded at different pump speeds and for both microsphere sizes were analyzed to obtain a relationship between the flow speed v in the main channel and Q. It was found that in all cases the speed of the microspheres was stabilized within 5 minutes after changing the pump speed. To be on the safe side, those measurements recorded 20, or 30 minutes after the change were used for further analysis. The average number of trajectories per series was 14, with a minimum of 2 and a maximum of 63. The values $v(Q)$ measured in the ramp-down series were equal within the error margin to the corresponding values from the ramp-up series, and were, therefore, averaged to obtain the speed for one pump setting and microsphere size. The error in the value of Q was estimated to be 10%. The error (standard deviation) in v was 27% and 31% for the larger and smaller microspheres, respectively. From the control experiment with no flow, we determined respective values of 0.26 and 1.6 μm/s.

Electron Microscopy Experiments

After determining that the system functioned as expected, we were able to test the results with even smaller particles in the STEM. In the STEM experiments, streaks appeared in the images several minutes after starting the pump. One of the acquired images is shown in Figure 10.

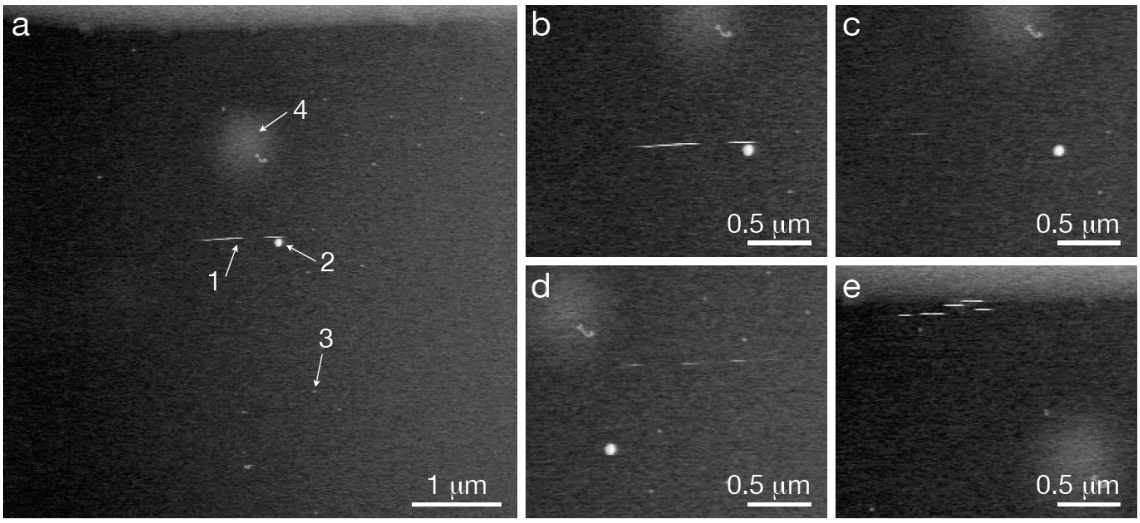

Figure 10 Liquid STEM imaging of flowing gold nanoparticles. (a) Image from a time-lapse imaging series recorded while flowing liquid containing 30 nm and 100 nm diameter gold nanoparticles in a 10% PBS buffer, with at a magnification of 24,000. Arrow #1 points towards a series of four streaks indicating a flowing gold nanoparticle. Arrow #2 and #3 indicate a 100 nm and a 30 nm gold nanoparticle, respectively. Arrow #4 is at the position of contamination of the window. (b) Close-up of the 4 streaks of image (a). (c) Image at the same position of (b), but recorded 17 seconds later. A single streak is visible. (d) Image showing three streaks close to the shape at arrow #4 in (a) and recorded 4 seconds after (a). (e) Pattern of 5 streaks above the shape at arrow #4 in image (a) recorded 13 seconds after (a). [27]

Figure 10a shows an image recorded after several minutes of flow. Four streaks are visible at arrow #1. At arrow #2 a stationary 100 nm gold nanoparticle, which was deposited on the silicon nitride window during flow, is visible. About twenty individual 30 nm diameter gold nanoparticles can be recognized (one is at arrow #3), as well as two clusters of 30 nm nanoparticles. A bright round shape is visible at arrow #4. This shape is probably contamination deposited on top of the window while parking the electron beam when the microscope was switched into recording mode. The brighter area at the top of the image was the edge of the flow cell. The appearance of moving and stationary nanoparticles on an initially clean window confirms that flow of liquid containing nanoparticles occurred through the microfluidics system during STEM imaging.

Figure 10b is a close-up of the streaks at arrow #1 in Figure 10a. Each streak was 1 pixel wide and was on average 0.18 μm long as determined from the full width at half maximum (FWHM) of a horizontal line-scan. The four streaks were on adjacent lines and each shifted to the left (starting from the top streak). The total shift was 0.78 μm, giving an average shift of 0.26 μm going from one line to the next. The speed of the nanoparticle was determined to be v = 0.1 mm/s by division by the line time. The signal intensity of the streaks was similar to that of the stationary 100 nm nanoparticle and we thus propose that the streaks were caused by a moving 100 nm nanoparticle. The FWHM over the stationary nanoparticle was 0.08 μm.

The next frame of the movie did not contain streaks, however, thirteen frames later a single streak was visible at the same position (Figure 10c). Figure 10d shows three streaks of intensity comparable to a 30 nm nanoparticle with an average FWHM of 0.1 μm. The streaks "skipped" one line. The shift was 0.28 μm/line and the speed was thus 0.1 mm/s, the same as the larger nanoparticle in Figure 10b. In Figure 10e, five streaks are visible, but the third streak is shifted in the opposite direction of the others.

A total of eight particles showing streaks shifted in the left direction were analyzed. The average travel distance was 0.31 ± 0.09 μm/line, which corresponds to a speed of v = 0.12 ± 0.03 mm/s. The speed was also checked by measuring the spread of the signal in the x direction for each particle captured. Assuming the brightest particles were 100 nm, the average spread of 16 measured particles was 53.3 nm, however the standard deviation of this measurement was quite large: $\pm$ 38.7 nm. This measurement showed an average particle speed of .76 $\pm$ .42 mm/s, which is on the same order of

magnitude as the speed obtained by measuring the traveling distance of the particles in the x and y directions.

These results demonstrate that nanoparticles can be injected into the specimen region of the liquid STEM during STEM operation, and that liquid STEM is capable of imaging moving gold nanoparticles in liquid flow. But, the direction of the flow has to be aligned with the scan direction in such way that two successive lines can capture the same particle. The speed captured here was on the order of 0.1 mm/s. The settings of the microscope (magnification, pixel dwell time, and image size) can be adjusted for a specific range of speeds to be captured.

CHAPTER V

DISCUSSION

Several lessons can be learned from the results of the experiments performed. Testing the cell growth conditions gave insight into the best way to grow the cells on the chips before starting any experiments. The LM experiments confirmed that the parallel-resistor model sufficiently describes the flow through the microfluidic system. It also provides important information about how the dimensions of the device can affect the results of the flow through the system. The STEM experiments further serve to confirm the model that was developed, as well as showing a first glimpse of moving particles in liquid in an electron microscope.

Cell Seeding Experiments

The results from the experimentation of how to grow the cells on the chips shows that the coatings and cleaning methods do not affect cell growth. If one wanted to grow the cells on the chips using this method, there is no advantage to coating the Petri dish with Pluronics. However, the results from the calculation of the media requirements for the cells show that the fewer cells present on the chips, the less media required. Because of this, it is preferable to pipette a small number of cells onto the chips, rather than to grow the cells directly on the chips in a Petri dish.

Light Microscopy Experiments

In the LM experiments, after the pump started it took about 4 minutes for the microspheres to reach the sample region at the SiN window, which is longer than the predicted time of one minute. However, this was in the case of initial zero flow, and it should be recalled that to establish flow with this system and pump takes several minutes. The injection speed can be increased by including a valve for injection during flow.

The results shown in Figure 9d indicate that the flow speed of both sizes of microspheres was equal and responded linearly to changes in the pump speed, within the error margin. Assuming that the speed of the microspheres is a measure of the speed of a liquid front in the main channel—thus neglecting Brownian motion—it follows from these results that the liquid flow speed in this microfluidic system is proportional to the pump speed. The deviations of the trajectories can be explained on the basis of Brownian motion that was evidently present, as was seen in the control data recoded in static liquid (Figure 9c). For both particle sizes, the measured mean squared displacement was smaller than the theoretical prediction by at most a factor of 2.6, and follow the predicted trend of an increase in x for smaller sizes.

The corresponding theoretical flow speed is also included in Figure 9d. As a first order approximation we can thus use the two-resistor model of Equation (10) to predict the behavior of the microfluidic system for STEM. A calculation of particular importance is the effect that changes in the dimensions of the specimen holder or microchips has on the speed of the liquid flow. If the bypass channel depth changed by 10 μm, (within manufacturing tolerances) v could change by up to 76%!

These results show that while the model is a valid way to describe the system, one must take care that all of the dimensions are accurate before relying on the model. On the other hand, this large variety in flow speed based on only small changes in one dimension of the system highlights the possibility in the future to alter certain dimensions only a small amount, in order to increase or decrease a desired variable.

Electron Microscopy Experiments

In the STEM experiments, the streaks measured (See Figure 10b) presumably represent a single gold nanoparticle moving to the left. We cannot fully rule out, however, that the four streaks may have been caused by a moving cluster of gold nanoparticles. A single streak (Figure 10c) could be caused by a nanoparticle traveling vertically with respect to the reference frame of the image. Any direction reversals can be explained by Brownian motion and charging effects. Charging effects may be more likely to cause directional changes like that seen in Figure 10e, as Brownian Motion would only be expected to cause a particle to move about .02 μm in the time that this particle appeared to actually move about .25 μm. The contribution of the charging effects to the direction and speed of the particles is unknown, and needs further examination.

The speed determined from STEM imaging is a factor of twelve larger than that found from the light microscopy experiments for the same pump speed. This difference can be explained by the following:

1) The depth of the bypass channel in the STEM could have been different than for the light microscopy experiment, for example, because the microchips were not

properly aligned in the slot, leaving a smaller gap, or because the microchips differed in size (within the 10 μm tolerance). The depth of the bypass channel would have to be d_b = 22 μm for the measured speeds to match the predicted speeds from the model. This value is not unrealistic and is actually close to the minimal distance measured between the alignment pole and the microchip of 30 μm.

2) Brownian motion may have caused the nanoparticles to speed up. Equation (11) predicts x = 158 nm for a 100 nm diameter nanoparticle in an interval of 2.6 ms (the line time of the STEM). From this number it can be expected that the observed particle movements contained a large component of Brownian motion, where the scanning direction may have selected nanoparticles moving in horizontal direction in Figure 10. Nanoparticles of larger sizes and liquids with higher viscosities can be used to reduce the effect of the Brownian motion of the STEM experiments.

3) Equation (10) was based on a two resistor model, while the system would act more like a three-resistor system if the microchips remain in the middle of the slot.

4) Other effects may have played a role, such as interaction of the electron beam with charged nanoparticles, the slowing of the liquid close to the surface [30] , or changes of the flow path due to bulging of the SiN windows.

Because STEM imaging of moving particles in liquid is so novel, although the motion of the particles cannot be fully explained by the data presented here with complete certainty, these images are an essential step towards the goal of high resolution imaging of dynamic systems in electron microscopy.

CHAPTER VI

CONCLUSION

In this thesis I have presented the design of the liquid STEM microfluidic system, including the microchips and the liquid flow specimen holder, which allows for the imaging of high-Z labels in a whole eukaryotic cell in liquid with nanometer resolution. I have also described the methods used to grow cells on the microchips. I have described results obtained by imaging the flow of microspheres in liquid through the system using light and electron microscopy, and how those results fit with mathematical models.

We found that the flow speed in the main channel of the microfluidic system responded linearly to changes in the pump speed as expected on the basis of a simple model of the flow through two parallel channels. The observed speeds were consistent with calculated values using the dimensions of the system. Despite the presumed large contribution of Brownian motion to the flow characteristics observed in the STEM, the results demonstrate that liquid STEM is capable of imaging moving gold nanoparticles when the direction of the flow is aligned with the scan direction in such way that two successive lines can capture the same particle.

For applications in biology a key feature of this system is the achievement of liquid flow during STEM imaging. Liquid flow removes free electrons, radicals, and excessive heat, that may be formed during STEM imaging. The liquid flow is also needed to provide nutrients when the system is used to image live cells. The rapid (within a minute) liquid exchange that is possible on account of the bypass channel

allows chemicals or ligands to be injected from the outside of the electron microscope into the sample region of the microfluidic system, which can be used to investigate the response of cells to stimuli.

CHAPTER VII

FUTURE DIRECTIONS

While the described system, has already shown the ability to image gold nanoparticles in whole eukaryotic cells with nanometer resolution, and the theoretical flow characteristics have been show to match with the experimental flow rates though the system, there are nonetheless some improvements that could be made. In the future, changes could be made to the model and/or device to make the mathematical characterization of flow more precise, and changes could be made to the device to maximize the length of time that cells could live in it.

There may be other, more precise models that could be employed to characterize the flow in the microfluidic system. Our previous results have shown that using the two resistor in parallel model provides results within a factor of ten, but the model could possibly be refined to improve upon this. Some possible improvements would be to try a three resistor in parallel model (considering that perhaps the chips are in the middle of the flow channel), or to model the system with two or three resistors in parallel, where the bypass resistor(s) consisted of several resistors in series (taking into account that the depth of the bypass channels is not consistent). The models and corresponding resistor networks are shown in Figure 11.

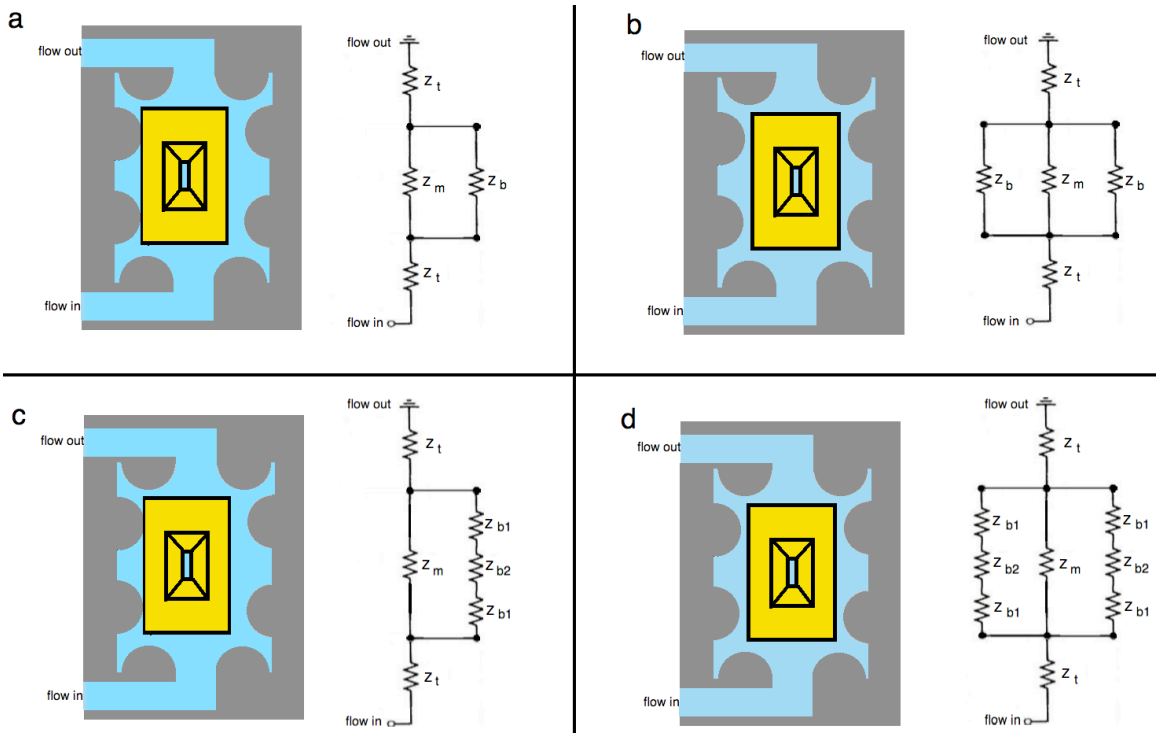

Figure 11 Possible models, shown in order of increasing complexity. (a) Simple two resistor model. Shown to fit experimental results within a factor of 10. (b) Simple three resistor model, considering that the chips may be between two channels. (c) Complex two resistor model, considering that the chips are pushed to one side of the holder, but also accounting for the change in depth of the bypass channel. (d) Complex three resistor model, considering that the chips may be between two channels, and also accounting for the change in depth of the bypass channels. Z is the resistance, and the subscript represents: t=tubing, m=main channel, b=bypass channel, b1 = bypass channel region 1, b2 = bypass channel region 2.

Part of trying to match the model to the precise dimensions of the system could include altering the dimensions of the holder to more easily match the model. This could include changes to the alignment poles, or perhaps even removing alignment poles on at least one side.

Furthermore, the dimensions of the entire system could be altered such that the experimental results fit more closely with the mathematical model. Preliminary results show that theoretically increasing the bypass channel depth, width and total length, while decreasing main channel depth and width (as well as the overall input flow rate) should lead to a closer fit between the experimental and theoretical results. Optimizing these

values could lead to a better fit for the model. The results of changing the dimensions are summarized in Figure 12.

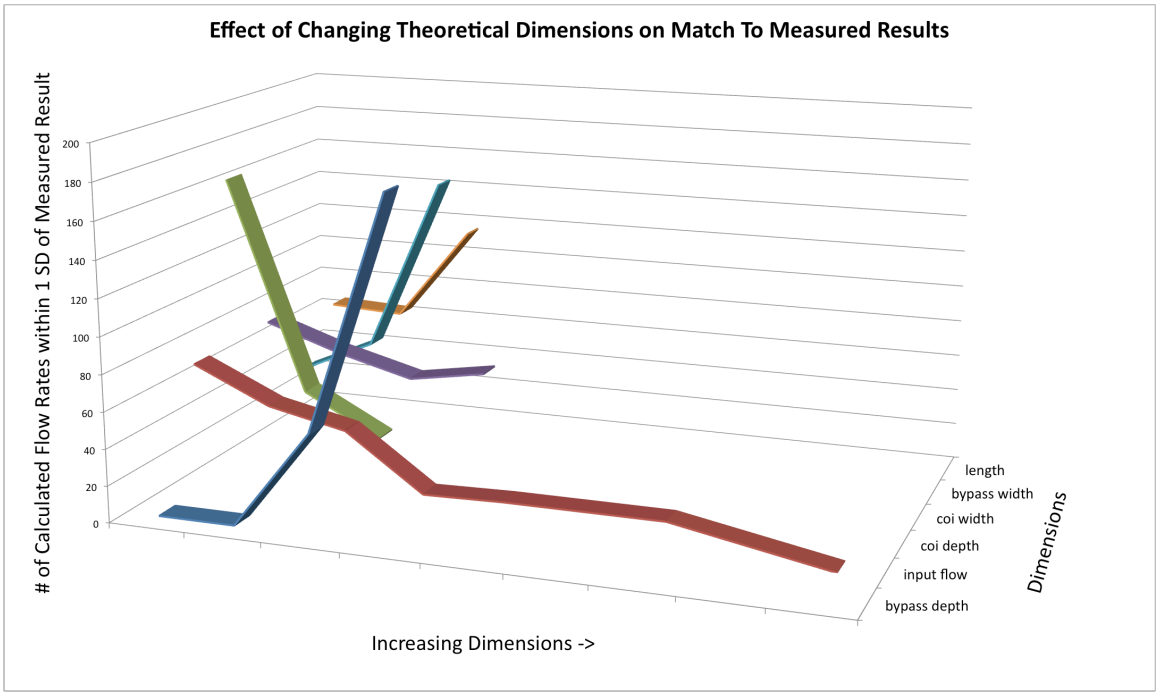

Figure 12 Graph showing how increasing various dimensions affects how often the final result is within one standard deviation of the experimental results.

Changing the dimensions to improve characterization could also serve to encourage cell growth. Because there is an upper limit to the flow rate that the device can tolerate, the only other ways to provide more fresh media for cells is increasing the dimensions of the main channel, altering the content of the media, and/or altering the windows such that they could support a higher flow rate. When optimizing the dimensions of the chips to provide the highest amount of media to the cells at all times, it is important to keep the dimensions small enough such that the flow can still be described as laminar, and one may still benefit from the microfluidic properties of the device, such as minimization of expensive chemicals used, and the similarity to the native state of the cells. Furthermore,

the thickness must always be minimized to improve imaging resolution.

While those precautions could ensure that the cells were as healthy as possible prior to STEM imaging, we are also investigating the addition of antioxidants and other protective agents, to the media to mitigate radiation damage to the cells [33], which may keep them alive during the STEM imaging itself. The rate of the flow could also be altered, which may require changing the dimensions of the windows to improve strength. One option would be to experiment with windows that are thicker in some areas for strength, and thinner in others for enhanced imaging capability. Another option would be instead of etching away one window from the silicon, etching several smaller windows. Although one must take care to ensure there is still enough of the window visible to obtain useful information from the LM images

Once the system is fully optimized, it will become an essential tool for Correlative Light and Electron Microscopy (CLEM). CLEM is accomplished by labeling cells with materials that are visible in both light and electron microscopes, such as gold nanoparticles, or high-Z particles known as Quantum Dots (QDs), which are visible in LMs by emitting fluorescence, where the color varies with the size of the particle, and are also visible in STEM due to their high atomic number [34].

Because cells will be able to live in the device prior to STEM imaging, it will be possible to image a sample in the LM, and then transfer it to the STEM at a particular timepoint and obtain a "snap shot" at that timepoint with nanometer resolution. After the "snap shot" the cell will likely be damaged from radiation from the electron beam. However, by taking "snap shots" at different timepoints (with different samples if necessary) during a dynamic event, one may compile these images together to obtain a

nanometer resolution movie of a dynamic event. In this way, we can get a general idea of what is happening during the event from the live imaging in the LM, and then zoom in to see particular labled proteins of interest in the high-resolution EM image. An example of CLEM imaging is shown in Figure 13.

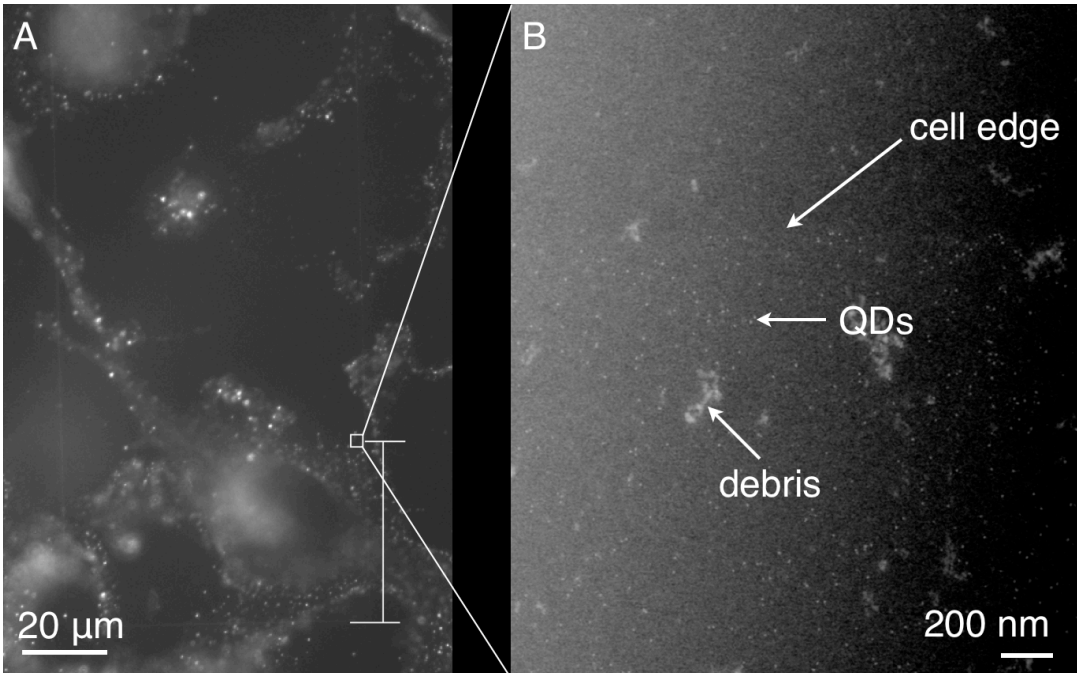

Figure 13 Correlative fluorescence microscopy and liquid STEM of intact fixed eukaryotic cells in saline water. (A) Fluorescence image of microchip with COS7 cells showing the regions with EGF labeled with Quantum Dots (QD) (B) Liquid STEM image of region indicated with square in (A). Individual QDs and the edge of the cell can be discerned. Some debris is also visible. [35]

One example where this imaging technique would be useful is to use liquid STEM and/or CLEM to examine the binding dynamics of Epidermal Growth Factor (EGF) to the Epidermal Growth Factor Receptor (EGFR). It is accepted that EGFR can exist as a monomer or homodimer in the plasma membrane. However, controversy exists as to whether the EGF ligand binds to an EGFR monomer causing dimerization, the ligand binds directly to preformed EGFR homodimers, or the ligand binds to both monomers and homodimers with a different affinity for each. Furthermore, the stoichiometry and allosteric regulation of the binding remain unclear [36].

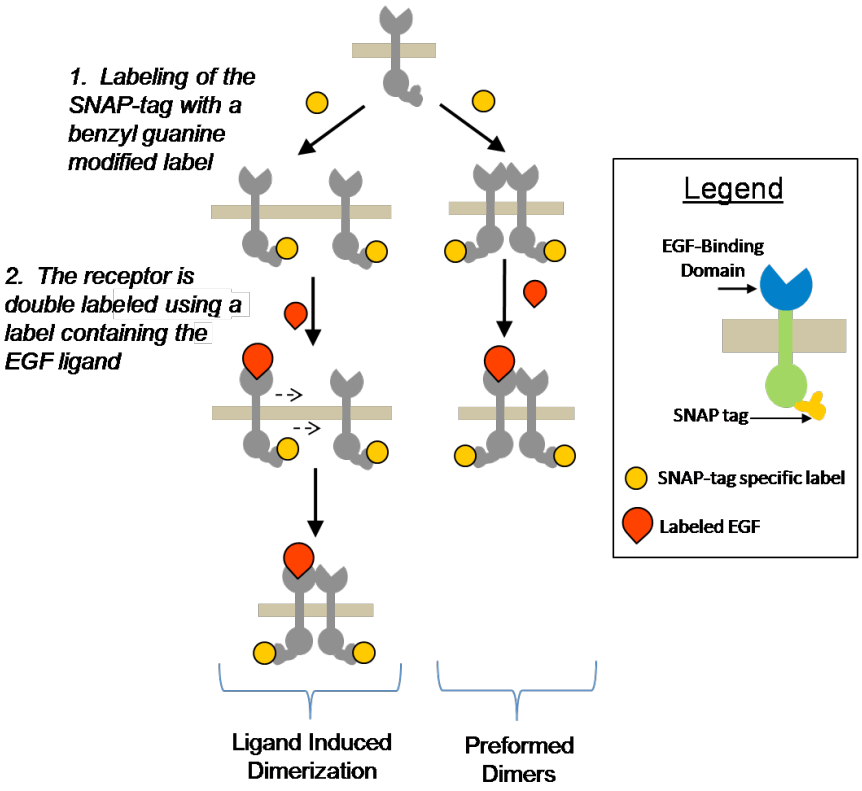

Figure 14 Two examples of possible binding dynamics of EGF and EGFR, ligand-induced dimerization is illustrated on the left, and ligand binding to preformed dimmers is shown on the right.

The intracellular portion of a transmembrane protein in a live cell can be modified with a so called SNAP tag, which allows nearly any label that has been modified to include a benzyl guanine molecule (including gold nanoparticles or QDs) to be attached to the protein of interest [37] (ie EGFR). Thus, using Liquid STEM, each individual labeled EGFR monomer can be imaged. The EGF ligand can also be modified with a distinct label (perhaps a gold nanoparticle or QD of another size or shape).

With the ability to image high-Z nanoparticles in whole eukaryotic cells with nanometer resolution, paired with the ability to inject a labeled ligand into a sample while imaging, one could image eukaryotic cells in liquid in the STEM before and after the

binding of labeled-EGF to labeled-EGFR, to directly visualize both the state of the receptor before and after binding, as well as the stoichiometry of the ligand and receptor after binding. We anticipate that this data will explain the binding dynamics and any allosteric regulation that may occur.

The resolution provided by liquid STEM in a correlated microscopy experiment will allow for unprecedented investigation into many dynamic *in vivo* processes, such as examining protein-protein interactions, and membrane organization and dynamics. Because the device is compatible with existing and future electron microscopes, it has the potential to become a new standard for molecular level imaging of live cells.

REFERENCES

1. Lippincott-Schwartz, J., E. Snapp, and A. Kenworthy, *Studying protein dynamics in living cells.* Nat Rev, 2001. **2**: p. 444-456.

2. Abbe, E., *Gesammelte Abhandlungen*. Vol. 2. 1904, Jena: Fisher, G.

3. Hecht, E., *Optics*. 4 ed. 2002, San Francisco, CA: Pearson Higher Education.

4. Hell, S.W., *Far-field optical nanoscopy.* Science, 2007. **316**: p. 1153-1158.

5. Hell, S.W. and J. Wichmann, *Breaking the diffraction resolution limit by stimulated emission: stimulated-emission-depletion fluorescence microscopy.* Optics Letters, 1994. **19**: p. 780-782.

6. Rust, M.J., M. Bates, and X. Zhuang, *Sub-diffraction-limit imaging by stochastic optical reconstruction microscopy (STORM).* Nature Methods, 2006. **3**: p. 793-796.

7. Betzig, E., et al., *Imaging Intracellular Fluorescent Proteins at Near-Molecular Resolution.* Science, 2006. **313**(1642-45).

8. Kendrew, J.C., et al., *A Three-Dimensional Model of the Myoglobin Molecule Obtained by X-Ray Analysis.* Nature, 1958. **181**: p. 662-666.

9. Geerlof, A., et al., *The impact of protein characterization in structural proteomics.* Acta Crystallographica, 2006. **62**: p. 1125-1136.

10. *Basic Methods in Microscopy*, ed. D.L. Spector and R.D. Goldman. 2006, Cold Spring Harbor, NY: Cold Spring Harbor Laboratory Press.

11. Sali, A., et al., *From words to literature in structural proteomics.* Nature, 2003. **422**: p. 216-225.

12. Parsons, D.F., *Structure of Wet Specimens in Electron Microscopy.* Science, 1974. **186**: p. 407-414.

13. Thiberge, S., et al., *Scanning electron microscopy of cells and tissues under fully hydrated conditions.* Proc. Natl. Acad. Sci., 2004. **101**(10): p. 3346.

14. Williamson, M.J., et al., *Dynamic microscopy of nanoscale cluster growth at the solid-liquid interface.* Nature Materials, 2003. **2**: p. 532-536.

15. Kirk, S.E., J.N. Shepper, and A.M. Donald, *Application of environmental scanning electron microscopy to determine biological surface structure.* J. Microscopy, 2009. **233**: p. 205-244.

16. Daulton, T.L., et al., *In Situ Environmental Cell–Transmission Electron Microscopy Study of Microbial Reduction of Chromium(VI) Using Electron Energy Loss Spectroscopy.* Microscopy and Microanalysis, 2001. **7**: p. 470-485.

17. Liu, K.L., et al., *Novel microchip for in situ TEM imaging of living organisms and bio-reactions in aqueous conditions.* Lab Chip, 2008. **8**: p. 1915-1921.

18. Zheng, H., et al., *Observation of single colloidal platinum nanocrystal growth trajectories.* Science, 2009. **324**(5932): p. 1309-12.

19. Phillips, R., J. Kondev, and J. Theriot, *Physical Biology of the Cell*. 2009, New York, NY: Garland Science.

20. Crewe, A.V. and J. Wall, *A scanning microscope with 5 A resolution.* J. Mol. Biol., 1970. **48**: p. 375-93.

21. Reimer, L., *Transmission electron microscopy*. 1984, Heidelberg: Springer.

22. Joy, D.C. and C.S. Joy, *Scanning electron microscope imaging in liquids – some data on electron interactions in water.* J. Micr., 2005. **221**: p. 84-99.

23. de Jonge, N., et al., *Electron microscopy of whole cells in liquid with nanometer resolution.* Proc. Natl. Acad. Sci., 2009. **106**: p. 2159-2164.

24. Xiao, Y., et al., *"Plugging into Enzymes": Nanowiring of Redox Enzymes by a Gold Nanoparticle.* Science, 2003. **299**: p. 1877-1881.

25. Nguyen, N.-T. and S.T. Werely, *Fundamentals and Applications of Microfluidics*. 2002, Norwood, MA: Artech House.

26. Walker, G.M., H.C. Zeringue, and D.J. Beebe, *Microenvironment design considerations for cellular scale studies.* Lab on a Chip, 2004. **4**: p. 91-97.

27. Ring, E.A. and N. de Jonge, *Microfluidic system for transmission electron microscopy.* Microscopy and Microanalysis, 2010. **in press**.

28. Nishiyama, H., et al., *Atmospheric scanning elecron microscope observes cells and tissues in open medium through silicon nitride film.* J Struct Biol, 2010. **in press**.

29. Longwell, P.A., *Mechanics of fluid flow*. 1966, New York: McGraw Hill.

30. Bao, J.B. and D.J. Harrison, *Measurement of Flow in Microfluidic Networks with Micrometer-Sized Flow Restrictors.* AIChE Journal, 2006. **52**(1): p. 75-85.

31. Easley, C.J., *Development and Application of Microfluidic Genetic Analysis Systems.* , in *Chemistry*. 2006, University of Virginia: Charlotsville.

32. Einstein, A., *On the Motion – Required by the Molecular Kinetic Theory of Heat – of Small Particles Suspended in a Stationary Liquid.* Annalen der Physik, 1905. **17**: p. 549-560.

33. Weiss, J.F. and M.R. Landauer, *Protection against ionizing radiation by antioxidant nutrients and phytochemicals.* Toxicology, 2003. **189**: p. 1-20.

34. Alivisatos, A.P., *Semiconductor Clusters, Nanocrystals, and Quantum Dots.* Science, 1996. **271**: p. 933-937.

35. de Jonge, N., et al. *Imaging Specific Protein Labels on Eukaryotic Cells in Liquid with Scanning Transmission Electron Microscopy*. in *Microscopy and Microanalysis*. 2010. Portland, OR.

36. Schlessinger, J., *Allosteric Regulartion of the Epidermal Growth Factor Receptor Kinase.* The Journal of Cell Biology, 1986. **103**(6): p. 2067-2072.

37. Keppler, A., et al., *A general method for the covalent labeling of fusion proteins with small molecules in vivo.* Nature Biotechnology, 2002. **21**: p. 86-89.